



OPEN

An efficient protocol for the synthesis of pyridines and hydroquinolones using IRMOF-3/GO/CuFe₂O₄ composite as a magnetically separable heterogeneous catalyst

Mohammad Ali Ghasemzadeh^{1✉}, Boshra Mirhosseini-Eshkevari¹ & Jaber Dadashi²

This study reports a facile and cost-effective technique for preparing magnetic copper ferrite nanoparticles supported on IRMOF-3/GO [IRMOF-3/GO/CuFe₂O₄]. The synthesized IRMOF-3/GO/CuFe₂O₄ was characterized with IR, SEM, TGA, XRD, BET, EDX, VSM, and elemental mapping. The prepared catalyst revealed higher catalytic behavior in synthesizing heterocyclic compounds through a one-pot reaction between various aromatic aldehydes, diverse primary amines, malononitrile, and dimedone under ultrasound irradiations. Among the notable features of this technique are higher efficiency, easy recovery from the reaction mixture, removal of a heterogeneous catalyst, and uncomplicated route. In this catalytic system, the activity level was almost constant after various stages of reuse and recovery.

Graphene oxide (GO) is a compound with surface or edge functional groups and superior chemical structures and features, making it an excellent support for various nanostructures^{1–4}. As graphene oxide has oxygen atoms in diverse isomers such as epoxide, carbonyl, carboxyl, and hydroxyl on its basal planes, various NPs can interact with GO sheets through charge-transfer interactions, physisorption, or electrostatic binding. This biodegradable nanostructure helps enhance the bioavailability of the nanocomposites and has some other advantages like high levels and thermal stability. GO acts as an anchoring support enabling uniform dispersion of the nanocomposites⁵.

In the last decade, nanoporous metal–organic frameworks (MOFs) comprising organic linkers and inorganic building units have been the subject of intense research⁶. This novel hybrid material includes a crystalline two or three and 1D open framework^{7–9}. MOF-based structures have unique features such as structural diversity, high porosity, high pore volume, and higher capacity for guest molecular acceptance¹⁰. MOFs are used in various fields like separation and storage of gases and as a catalyst^{11–13}. MOFs represent higher flexibility for designing catalytic centers than purely inorganic porous materials¹⁴. This flexibility makes them attractive substances for heterogeneous catalysts. There are several methods to modulate MOFs owing to the significant variety of metal ions and organic linkers. The appearance and size of the framework can be altered via different linkers and altering their connectivity by adding various functional groups on the linkers^{15,16}. Using metal–organic frameworks as green catalysts accelerates the organic reactions. As mentioned in the previous authoritative articles, the metal ions in the structure of MOFs act as a Lewis acid and the carboxylate anion as a Lewis base. In this respect, the IRMOF-3 structure has been used as a bifunctional catalyst in the IRMOF-3/GO/CuFe₂O₄ structure due to the presence of metal cation sites (Zn²⁺) and also carboxylate anions¹⁷. The existence of non-coordinated amino groups structure in IRMOF-3 demonstrates that the basicity of the aniline-like amino group is enhanced when incorporated inside the pores of MOF channels.

Using multi-component reactions (MCRs) as an organized and efficient method has caused a revolution in designing novel approaches and creating multifarious chemical libraries with molecular diversity in the last

¹Department of Chemistry, Qom Branch, Islamic Azad University, Post Box, Qom 37491-13191, Iran. ²Catalysts and Organic Synthesis Research Laboratory, Department of Chemistry, Iran University of Science and Technology, Tehran 16846-13114, Iran. ✉email: m.a.qasemzade@gmail.com

decade. They have specific features such as higher atomic economy, straightforward reaction model, shorter reaction time, and conformity with other green chemistry principles. Hence, these chemical reactions have become the most potent and prevailing approach to synthesizing heterocyclic compounds¹⁸. Recently, numerous studies have been conducted on developing novel synthetic techniques to synthesize quinoline and pyridine compounds. This high attention is attributed to their promising and notable diversity in pharmacological and therapeutic activities like geroprotective, antitubercular, anticancer, antidiabetic, and analgesic activities¹⁹. Different developed synthetic approaches and catalysts, such as LiBr, CTAB, CuBr, salicylic acid, *L*-proline, and GO nanoparticles^{20–25}, have been proposed to synthesize these biological and chemical molecules. However, they mostly encounter some disadvantages and negative points such as applying impotent and inefficient catalysts, low yield of the products, difficult reaction conditions, and tedious work-up procedures. Thus, designing and providing novel synthetic methods for these biological molecules is challenging.

The present study aims to enhance more effective synthetic procedures, lower the number of isolated reaction stages, and minimize wastes by preparing the heterocyclic compounds^{26–28}. Next, we report a new and mild route for synthesizing heterocyclic compounds through a one-pot reaction between various aromatic aldehydes, diverse primary amines, malononitrile, and dimedone under ultrasound irradiations in the attendance of IRMOF-3/GO/CuFe₂O₄ nanocatalyst (Fig. 1).

Experimental

Preparing CuFe₂O₄ nanoparticles. A solution of FeCl₂·4H₂O and CuCl₂·2H₂O (molar ratio, 2:1) in deionized water (30 mL) was added to a concentrated solution of NaOH to reach a pH of 13. Then, the mixture was stirred vigorously at 70 °C until to formation of a black residue, including CuFe₂O₄. The precipitate was rinsed several times after cooling and dried overnight at 80 °C. Finally, it was calcinated for 5 h in a furnace at 700 °C.

Preparation of IRMOF-3/CuFe₂O₄ nanocomposite. A mixture of CuFe₂O₄ (0.05 g), Zn(NO₃)₂·6H₂O (0.066 g) and NH₂-BDC (0.016 g) was dissolved in DMF (10 mL) under vigorous stirring. Next, the solution was transferred to an autoclave and heated at 120 °C for 10 h. The precipitate was separated after cooling, by a simple filtration. The obtained crystals were then soaked in 20 mL of DMF at 80 °C for 12 h. Lastly, the obtained IRMOF-3/CuFe₂O₄ was dried for 24 h at 40 °C²⁹.

Synthesis of IRMOF-3/GO/CuFe₂O₄ nanocatalyst. In this research, our catalyst including IRMOF-3/GO/CuFe₂O₄ was successfully prepared according to the modified Hummer's method and our previously published paper^{30,31}, (See Supplementary Information, Fig. S1).

General synthesis of 2-amino-4-aryl-6-substituted pyridine-3,5-dicarbonitrile (4a-r) using IRMOF-3/GO/CuFe₂O₄ nanocatalyst. IRMOF-3/GO/CuFe₂O₄ nanocomposite (0.003 g) was added to a solution of aromatic amine (1 mmol), malononitrile (2 mmol), and aldehyde (1 mmol) in 5 mL of EtOH. The mixture was sonicated under ultrasonic irradiations (25 kHz frequency) for 10–20 min. After completing the reaction, the obtained solid was filtered, and the contents were dissolved in acetone, and the insoluble IRMOF-3/GO/CuFe₂O₄ nanocomposite was separated by centrifuge. In the last step, the solvent was evaporated under a vacuum, and the precipitate was recrystallized using ethanol to provide the corresponding 2-amino-4-aryl-6-substituted pyridine-3,5-dicarbonitrile.

General synthesis of hydroquinoline-3-carbonitrile derivatives (6a-d) in the presence of IRMOF-3/GO/CuFe₂O₄ nanostructure. A mixture of anilines (1 mmol), malononitrile (1.1 mmol), aldehyde (1 mmol), dimedone (2 mmol), and IRMOF-3/GO/CuFe₂O₄ (0.005 g) was added to a flask containing ethanol (5 mL). The mixture was sonicated for the appropriate times. The catalyst was separated over completion (monitored by TLC), by dissolving the obtained heterocyclic compounds in dichloromethane. Finally, the corresponding products in high purity were collected by evaporating the dichloromethane.

The scanned original spectral data of new compounds are provided in Supporting Information.

2-amino-4-(4-cyanophenyl)-6-((4-methoxyphenyl) amino) pyridine-3,5-dicarbonitrile 4j. Yellow solid; m.p. 223–225 °C. IR spectrum ν , cm⁻¹: 3365, 3172, 3051, 2932, 2370, 1705, 1674, 1591, 1458, 1205; ¹H NMR (250 MHz, DMSO-*d*₆): 3.84 (s, 3H, CH₃), 5.43 (s, 2 H, NH₂), 6.76–7.04 (d, 2H, *J*=8.2 Hz, ArH), 7.28–7.36 (d, 2H, *J*=8.3 Hz, ArH), 7.65–7.75 (m, 4H, ArH), 9.85 (s, 1H, NH); ¹³C NMR (62.9 MHz, DMSO-*d*₆) δ : 27.33, 31.39, 68.62, 76.82,

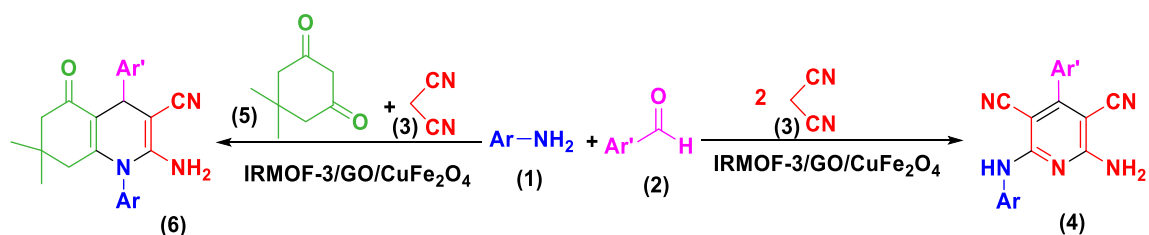


Figure 1. Synthesis of pyridines and quinolines using IRMOF-3/GO/CuFe₂O₄.

87.26, 101.03, 112.53, 123.45, 131.34, 133.43, 134.25, 138.56, 144.43, 146.33, 148.62, 156.47, 165.38, 168.28, 170.21, 183.31, 188.22; Anal. Calcd. For: C₂₁H₁₄N₆O: C 68.84, H 3.85, N 22.94. O 4.37. Found: C 76.88, H 3.82, N 22.92 O 4.35; MS (EI) (m/z): 366.12 (M⁺).

2-amino-6-((4-methoxyphenyl)amino)-4-(4-(methylthio)phenyl)pyridine-3,5 dicarbonitrile 4k. Yellow solid; m.p. 210–212 °C. IR spectrum ν , cm⁻¹: 3363, 3170, 2555, 21,381, 1701, 1678, 1593, 1458, 1377, 1207; ¹H NMR (250 MHz, DMSO-*d*₆): 2.36 (s, 3H, CH₃), 3.72 (s, 3H, CH₃), 5.48 (s, 2 H, NH₂), 6.76–7.04 (d, 2H, *J*=8.2 Hz, ArH), 7.27–7.36 (d, 2H, *J*=8.3 Hz, ArH), 7.65–7.78 (m, 4H, ArH), 9.82 (s, 1H, NH); ¹³C NMR (62.9 MHz, DMSO-*d*₆) δ : 28.39, 32.33, 67.62, 77.82, 86.26, 102.03, 113.52, 125.44, 132.34, 134.43, 136.26, 139.56, 146.44, 148.33, 149.69, 154.47, 162.34, 164.28, 171.21, 181.32, 187.21; Anal. Calcd. For: C₂₁H₁₇N₃OS: C 65.10, H 4.42, N 18.08. O 4.13, S 8.27. Found: C 65.14, H 4.45, N 18.04, O 4.316, S 8.25; MS (EI) (m/z): 387.12 (M⁺).

2-amino-4-(4-cyanophenyl)-1-(4-methoxyphenyl)-7,7-dimethyl-5-oxo-1,4,5,6,7,8 hexahydroquinoline-3-carbonitrile 6c. Yellow solid; m.p. 242–243 °C. IR spectrum ν , cm⁻¹: 3321, 3062, 2985, 2233, 1608, 1716, 1678, 1381, 1284; ¹H NMR (250 MHz, DMSO-*d*₆) δ : 0.82 (s, 3H, CH₃), 0.95 (s, 3H, CH₃), 2.29 (d, 2H, *J*=8.4 Hz, 2CH), 2.44 (d, 2H, *J*=8.2 Hz, 2CH), 3.82 (s, 3H, CH₃), 4.33 (s, 1 H, CH), 5.33 (s, 2 H, NH₂), 6.74–7.05 (d, 2H, *J*=8.6 Hz, ArH), 7.28–7.32 (d, 2H, *J*=8.3 Hz, ArH), 7.62–7.78 (m, 4H, ArH); ¹³C NMR (62.9 MHz, DMSO-*d*₆) δ : 28.33, 30.79, 78.61, 88.62, 92.24, 102.06, 117.46, 118.41, 124.54, 128.61, 130.54, 132.93, 133.22, 137.51, 142.63, 144.01, 149.32, 159.27, 166.88, 173.46, 178.81, 180.74, 183.31, 192.12, 194.81, 196.71; Anal. Calcd. For: C₂₆H₂₄N₄O₂: C 73.56, H 5.70, N 13.20, O 7.54. Found: C 73.54, H 5.73, N 13.24, O 7.52; MS (EI) (m/z): 424.19 (M⁺).

2-amino-1-(4-methoxyphenyl)-7,7-dimethyl-4-(4-(methylthio)phenyl)-5-oxo-1,4,5,6,7,8 hexahydroquinoline-3-carbonitrile 6d. Yellow solid; m.p. 256–258 °C. IR spectrum ν , cm⁻¹: 3352, 3186, 2962, 2191, 1685, 1651, 1604, 1369, 1211; ¹H NMR (250 MHz, DMSO-*d*₆): 0.84 (s, 3H, CH₃), 0.97 (s, 3H, CH₃), 2.28 (d, 2H, *J*=7.3 Hz, 2CH), 2.42 (d, 2H, *J*=7.8 Hz, 2CH), 2.78 (s, 3H, SCH₃), 3.83 (s, 3H, CH₃), 4.32 (s, 1 H, CH), 5.33 (s, 2 H, NH₂), 6.75–7.03 (d, 2H, *J*=8.3 Hz ArH), 7.27–7.38 (d, 2H, *J*=8.6 Hz, ArH), 7.64–7.75 (m, 4H, ArH); ¹³C NMR (62.9 MHz, DMSO-*d*₆) δ : 27.33, 31.72, 76.26, 85.62, 94.22, 104.06, 116.41, 119.46, 123.54, 126.81, 131.54, 133.93, 135.22, 138.51, 141.62, 143.01, 148.32, 157.24, 164.87, 175.44, 176.86, 182.71, 185.31, 193.11, 193.82, 195.71; Anal. Calcd. For: C₂₆H₂₇N₃O₂S: C 70.09, H 6.11, N 9.43. O 7.18, S, 7.20. Found: C 70.06, H 6.16, N 9.48 O 7.12, S, 7.24; MS (EI) (m/z): 455.18 (M⁺).

Results and discussion

IRMOF-3/GO/CuFe₂O₄ was successfully synthesized as mentioned in our previous study³¹. The structure of this catalyst was determined using EDX/Mapping, IR, and TGA analysis (See Supplementary Information, Figs. S2–S5)³¹, and also with other spectral techniques including SEM (Fig. 2), XRD (Fig. 3), BET (Fig. 4), and VSM (Fig. 5).

The microscopic morphology of the products was visualized by scanning electron microscopy (SEM). This analysis showed that CuFe₂O₄ is composed of relatively uniform quasispherical particles (Fig. 2a)³². SEM images of IRMOF-3 showed that this structure has a crystalline and rod shape, per previous reports (Fig. 2b)³³. SEM image of the GO shows the particles of GO look very dense with the layers stacked together due to dispersive forces and strong specific interactions between the surface groups on the graphene-like layers (Fig. 2c)³⁴. SEM images for the IRMOF-3/GO/CuFe₂O₄ nanocomposite are shown in Fig. 3d. As can be seen, the particles have regular and spherical shapes (Fig. 2d).

XRD pattern of the CuFe₂O₄ nanoparticles is shown in Fig. 3a. The peaks at 29.80°, 32.21°, 35.71°, 43.31°, 48.40°, 57.25°, 59.66° and 63.62° (2 θ) indicate the formation of the CuFe₂O₄ nanoparticles³⁵. Also the peaks at 8.4°, 9.6°, 13.7°, 15.35°, 19.39° and 24.62° (2 θ) show the presence of the IRMOF-3 frameworks (Fig. 3b)³⁶. Here, the peak at 2 θ = 11.1° indicates the creation of the GO (Fig. 3c)^{37,38}. Fig. 2d presents the XRD pattern of IRMOF-3/GO/CuFe₂O₄. The peaks observed at 2 θ = 29.80°, 32.21°, 35.71°, 43.31°, 48.40°, 57.25°, 59.66° and 63.62° are related to the CuFe₂O₄. Also, the peaks at 2 θ of 8.4°, 9.6°, 13.7°, 15.35°, 19.39°, and 24.62° show the presence of the IRMOF-3 frameworks, while the peak at 2 θ = 11.1° indicates the creation of the GO, confirming the formation of the nanocomposite. These results demonstrate that the crystalline structure of the CuFe₂O₄ and IRMOF-3 materials was unchanged and remained intact during the catalyst preparation.

Nitrogen adsorption/desorption isotherms were used to study the specific surface area and pore volume distribution of nanostructures including CuFe₂O₄, GO, IRMOF-3, and IRMOF-3/GO/CuFe₂O₄ by the Brunauer–Emmett–Teller (BET) approach (Fig. 4). The CuFe₂O₄ represented a BET surface area, total pore volume, and the average pore diameter of 34.65 m² g⁻¹, 0.138 cm³ g⁻¹, and 1.17 nm respectively. In comparison, these analyses for GO, IRMOF-3 and IRMOF-3/GO/CuFe₂O₄ gave values of 48.51 m² g⁻¹, 0.182 cm³ g⁻¹, and 1.24 nm, 884.82 m² g⁻¹, 0.887 cm³ g⁻¹, and 1.42 nm, and 456.29 m² g⁻¹, 0.435 cm³ g⁻¹ and, 1.65 nm, respectively (Fig. 4 and Table 1). The adsorption–desorption isotherm of all the four samples exhibits a reversible type-II adsorption isotherm, indicating the presence of micro- and macro-pores³⁹. The decreasing BET surface area and total pore volume can be attributed to incorporating of IRMOF-3/CuFe₂O₄ groups inside the pure GO. However, the open cavities and high surface areas were retained, which benefited the free dispersal of the reactant and product.

The so-called VSM analysis was further conducted to investigate the magnetic behavior of the IRMOF-3/CuFe₂O₄, and IRMOF-3/GO/CuFe₂O₄ nanocomposite, with the outcomes presented in Fig. 5. According to the results, the value of magnetic saturation was measured at 67.45, and 38.45 emu/g for the IRMOF-3/CuFe₂O₄ and IRMOF-3/GO/CuFe₂O₄ nanocomposite, respectively⁴⁰.

The performance of the prepared IRMOF-3/GO/CuFe₂O₄ nanocomposite was evaluated using the catalyst in the preparation of 2-amino-4-aryl-6-substituted pyridine-3,5-dicarbonitrile and hydroquinoline-3-carbonitrile

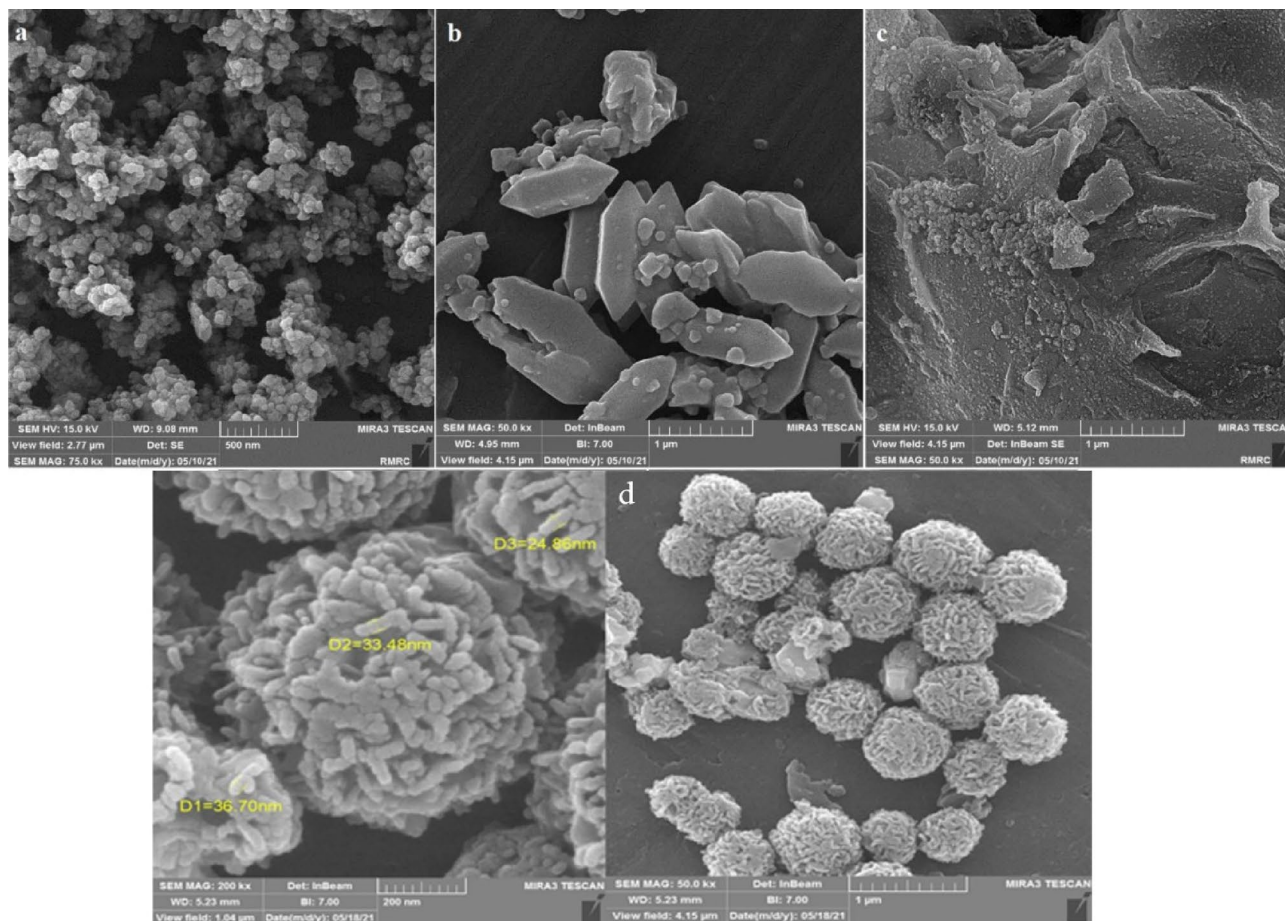


Figure 2. SEM analysis of (a) CuFe_2O_4 , (b) IRMOF-3, (c) GO, and (d) IRMOF-3/GO/ CuFe_2O_4 .

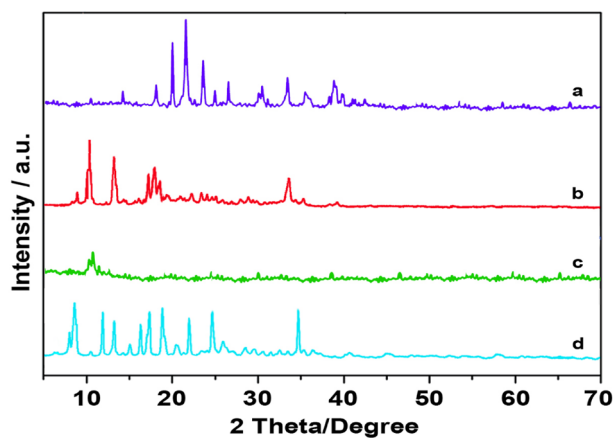


Figure 3. XRD patterns of (a) pure CuFe_2O_4 , (b) IRMOF-3, (c) GO, and (d) IRMOF-3/GO/ CuFe_2O_4 .

derivatives. To this end, a three-component reaction of 4-bromobenzaldehyde, *p*-toluidine, and malononitrile was chosen as a model study for synthesizing 2-amino-4-(4-bromophenyl)-6-(*p*-tolylamino)pyridine-3,5-dicarbonitrile (4e). In addition, the reaction of *p*-toluidine, 4-bromobenzaldehyde, dimedone, and malononitrile was considered a model reaction for the preparation of 2-amino-4-(4-bromophenyl)-7,7-dimethyl-5-oxo-1-(*p*-tolyl)-1,4,5,6,7,8-hexahydroquinoline-3-carbonitrile (6b) (Table 2). The model reactions were investigated by different conditions, including catalyst, solvent, and amount of catalyst.

Firstly, the preparation of compounds 4e and 6p was considered in the occurrence of different catalysts like Fe_3O_4 , CuFe_2O_4 , MgO, SiO_2 , IRMOF-3/ CuFe_2O_4 , CuI, GO, and IRMOF-3/GO/ CuFe_2O_4 nanostructures under ultrasound irradiations in EtOH as solvent (0.01 g of each catalyst was used). The best results were

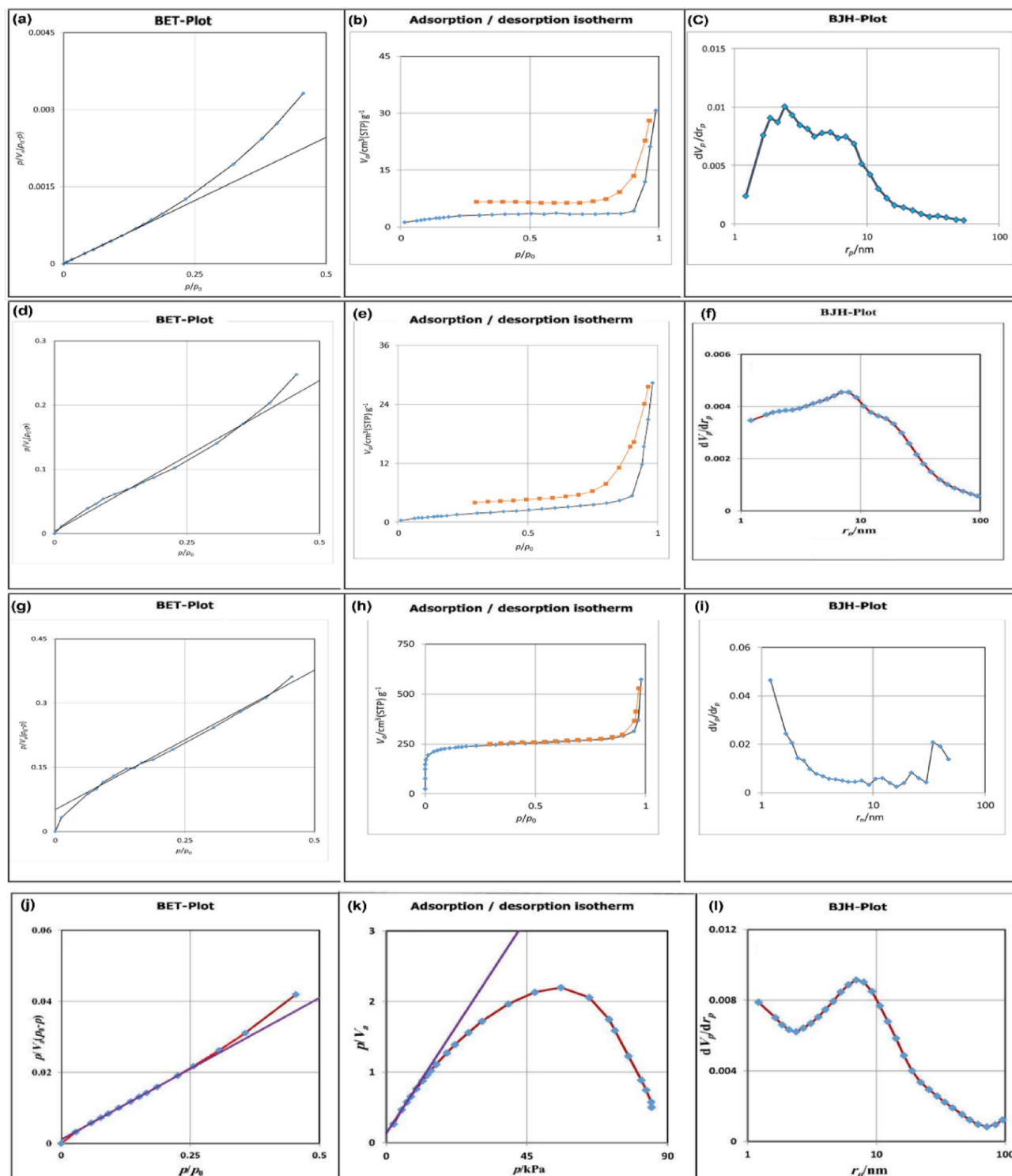


Figure 4. BET-plot of CuFe_2O_4 (a), adsorption/desorption of CuFe_2O_4 (b), BJH-plot of CuFe_2O_4 (c); BET-plot of GO (d), adsorption/desorption of GO (e), BJH-plot of GO (f); BET-plot of IRMOF-3 (g), adsorption/desorption of IRMOF-3 (h), BJH-plot of IRMOF-3 (i), BET-plot of IRMOF-3/GO/ CuFe_2O_4 (j), adsorption/desorption of IRMOF-3/GO/ CuFe_2O_4 (k), BJH-plot of IRMOF-3/GO/ CuFe_2O_4 (l).

obtained (Table 2), when using IRMOF-3/GO/ CuFe_2O_4 nanocomposite as catalyst (Table 2, entries 8 and 16). Afterward, it was tried to investigate the influence of various solvents like water, chloroform, dimethylformamide, ethanol, toluene, and solvent-free conditions in synthesizing of 2-amino-4-(4-bromophenyl)-6-(*p*-tolylamino)pyridine-3,5-dicarbonitrile (4e) in the presence of IRMOF-3/GO/ CuFe_2O_4 (0.01 g) (Table 2, entries 17–22).

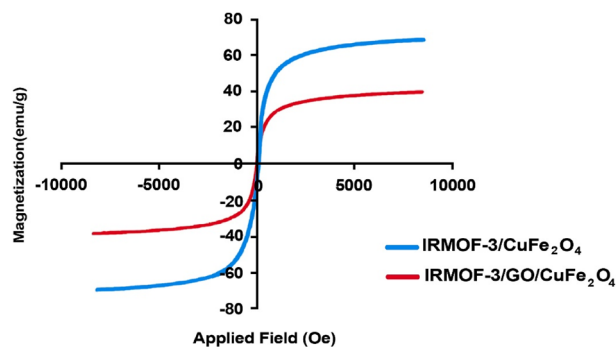


Figure 5. Magnetization curves of IRMOF-3/CuFe₂O₄ and IRMOF-3/GO/CuFe₂O₄.

| Sample | BET Surface area (m ² /g) | Pore volume (cm ³ /g) | Pore size (nm) |
|---|--------------------------------------|----------------------------------|----------------|
| CuFe ₂ O ₄ | 34.65 | 0.138 | 1.17 |
| GO | 48.51 | 0.182 | 1.24 |
| IRMOF-3 | 884.82 | 0.887 | 1.42 |
| IRMOF-3/GO/CuFe ₂ O ₄ | 456.29 | 0.435 | 1.65 |

Table 1. Measured BET surface areas and pore volumes of CuFe₂O₄, GO, IRMOF-3 and IRMOF-3/GO/CuFe₂O₄.

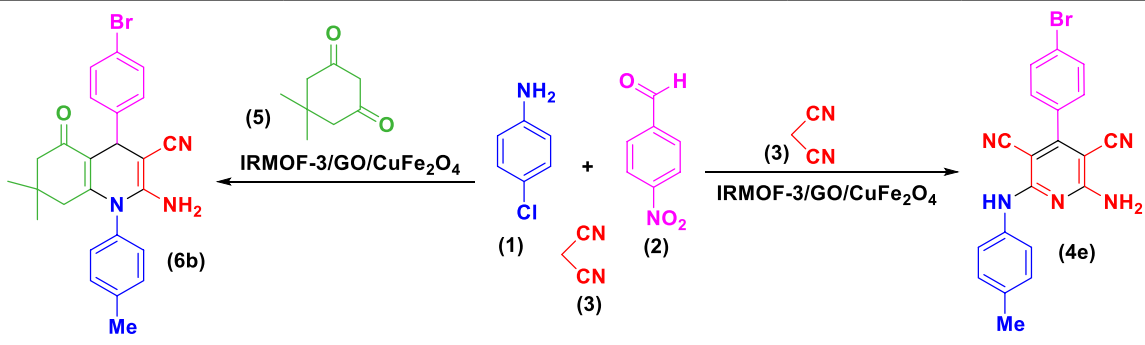
Table 2 shows no product was achieved without any solvent under ultrasonic irradiation. Furthermore, it was concluded that the presence of ethanol as solvent provided the best outcome considering reaction time and yield of the corresponding product. Subsequently, the preparation of hexahydroquinoline-3-carbonitrile (6b) was also examined using different polar and nonpolar solvents (Table 2, entries 23–28). As indicated in this Table 2, using EtOH as solvent provided the best reaction conditions (Table 2, entries 20 and 26).

In the next stage, it was decided to assess the optimum amount of the nanocatalyst for preparing of 4e and 6b. Different amounts of the catalyst were used for preparing 2-amino-4-(4-bromophenyl)-6-(*p*-tolylamino)pyridine-3,5-dicarbonitrile and 2-amino-4-(4-bromophenyl)-7,7-dimethyl-5-oxo-1-(*p*-tolyl)-1,4,5,6,7,8-hexahydroquinoline-3-carbonitrile (Table 3). The model was run using various amounts of the catalyst from 0.001 to 0.007 g. Eventually, the optimal amounts were found to be 0.003 and 0.005 g for compounds 4e and 6p, respectively.

Some aromatic aldehydes and amines were used to investigate the catalytic efficiency and performance of the IRMOF-3/GO/CuFe₂O₄ on synthesizing various pyridine and hydroquinoline derivatives under optimized reaction conditions. After conducting some experiments, we obtained some 2-amino-4-aryl-6-substituted-pyridine-3,5-dicarbonitriles and hydroquinolone-3-carbonitriles in good to excellent yields within short reaction times. As illustrated in Table 4, different aldehydes and anilines with various substituents could participate in the multi-component synthesis of corresponding heterocyclic compounds. However, as indicated, benzaldehydes with electron-withdrawing groups reacted faster than electron-donating ones. Moreover, the aromatic amines having electron-releasing groups reacted faster than anilines containing electron-withdrawing groups. According to the mechanism pathway, the first step of the mechanism is the Knoevenagel condensation between malononitrile and aromatic aldehyde. Obviously, the presence of electron-withdrawing groups on the benzaldehydes leads to a faster reaction due to more electrophilicity of the carbon group of the carbonyl^{41,42}. While using IRMOF-3/GO/CuFe₂O₄ as a catalyst serves as a Lewis acid catalyst and increases the electrophilicity of the carbonyl groups of aldehydes. The synergic effects of both electron-withdrawing groups and Lewis acidity of IRMOF-3/GO/CuFe₂O₄ increase the reaction rate. Nevertheless, against the electron-withdrawing groups, the existence of electron-donating groups lowers the speed of the reaction, because of a slower nucleophilic attack on carbonyl groups of aldehydes.

The catalyst efficiency and usability for synthesizing 2-amino-4-aryl-6-substituted pyridine-3,5-dicarbonitrile and hydroquinoline-3-carbonitrile derivatives were compared with those of some previously reported catalysts. As presented in Table 5, IRMOF-3/GO/CuFe₂O₄ is better than previously reported catalysts in saving time, and energy, and excellent yields of the products (Table 5).

Reuse of catalyst. In this research, the reusability of IRMOF-3/GO/CuFe₂O₄ composite was investigated for the three-component reaction of 4-bromobenzaldehyde, *p*-toluidine, and malononitrile (compound 4e). Upon completion of the reaction, the IRMOF-3/GO/CuFe₂O₄ nanostructure was separated using a centrifuge instrument and washed with dichloromethane. The obtained recovered catalyst was dried at 40 °C for 24 h. As indicated in Fig. 6, the recovered catalyst could be used 7 times. Furthermore, the XRD technique was used to demonstrate the efficiency and consistency of the rescue IRMOF-3/GO/CuFe₂O₄ after seven runs uses. As



| Entry | Compound | Solvent | Catalyst | T (°C) | Time (min) | Yield% |
|-------|-----------|-------------------------------------|---|------------|------------|-----------|
| 1 | 4e | C ₂ H ₅ OH | Fe ₃ O ₄ NPs | u.s | 25 | 68 |
| 2 | 4e | C ₂ H ₅ OH | CuFe ₂ O ₄ NPs | u.s | 25 | 70 |
| 3 | 4e | C ₂ H ₅ OH | MgO NPs | u.s | 35 | 75 |
| 4 | 4e | C ₂ H ₅ OH | SiO ₂ NPs | u.s | 45 | 65 |
| 5 | 4e | C ₂ H ₅ OH | IRMOF-3/CuFe ₂ O ₄ | u.s | 25 | 85 |
| 6 | 4e | C ₂ H ₅ OH | CuI NPs | u.s | 30 | 75 |
| 7 | 4e | C ₂ H ₅ OH | GO NPs | u.s | 35 | 80 |
| 8 | 4e | C₂H₅OH | IRMOF-3/GO/CuFe₂O₄ | u.s | 15 | 92 |
| 9 | 6b | C ₂ H ₅ OH | Fe ₃ O ₄ NPs | u.s | 35 | 80 |
| 10 | 6b | C ₂ H ₅ OH | CuFe ₂ O ₄ NPs | u.s | 40 | 82 |
| 11 | 6b | C ₂ H ₅ OH | MgO NPs | u.s | 60 | 55 |
| 12 | 6b | C ₂ H ₅ OH | SiO ₂ NPs | u.s | 45 | 65 |
| 13 | 6b | C ₂ H ₅ OH | IRMOF-3/CuFe ₂ O ₄ | u.s | 30 | 72 |
| 14 | 6b | C ₂ H ₅ OH | CuI NPs | u.s | 35 | 75 |
| 15 | 6b | C ₂ H ₅ OH | GO NPs | u.s | 40 | 78 |
| 16 | 6b | C₂H₅OH | IRMOF-3/GO/CuFe₂O₄ | u.s | 25 | 90 |
| 17 | 4e | H ₂ O | IRMOF-3/GO/CuFe ₂ O ₄ | u.s | 35 | 75 |
| 18 | 4e | CHCl ₃ | IRMOF-3/GO/CuFe ₂ O ₄ | u.s | 45 | 45 |
| 19 | 4e | DMF | IRMOF-3/GO/CuFe ₂ O ₄ | u.s | 35 | 75 |
| 20 | 4e | C₂H₅OH | IRMOF-3/GO/CuFe₂O₄ | u.s | 15 | 92 |
| 21 | 4e | PhCH ₃ | IRMOF-3/GO/CuFe ₂ O ₄ | u.s | 45 | 40 |
| 22 | 4e | – | IRMOF-3/GO/CuFe ₂ O ₄ | u.s | 45 | -- |
| 23 | 6b | H ₂ O | IRMOF-3/GO/CuFe ₂ O ₄ | u.s | 60 | 65 |
| 24 | 6b | CHCl ₃ | IRMOF-3/GO/CuFe ₂ O ₄ | u.s | 60 | 50 |
| 25 | 6b | DMF | IRMOF-3/GO/CuFe ₂ O ₄ | u.s | 45 | 65 |
| 26 | 6b | C₂H₅OH | IRMOF-3/GO/CuFe₂O₄ | u.s | 25 | 90 |
| 27 | 6b | PhCH ₃ | IRMOF-3/GO/CuFe ₂ O ₄ | u.s | 60 | 35 |
| 28 | 6b | – | IRMOF-3/GO/CuFe ₂ O ₄ | u.s | 60 | -- |

Table 2. The influence of various catalysts and solvents in the preparation of 4e and 6b compounds. Significant values are in bold.

| Entry | Compound | Catalyst (g) | Time (min) | Yield % |
|-------|-----------|--------------|------------|-----------|
| 1 | 4e | 0.001 | 30 | 70 |
| 2 | 4e | 0.002 | 25 | 85 |
| 3 | 4e | 0.003 | 15 | 92 |
| 4 | 4e | 0.005 | 15 | 92 |
| 5 | 6b | 0.001 | 60 | 55 |
| 6 | 6b | 0.002 | 45 | 75 |
| 7 | 6b | 0.003 | 40 | 85 |
| 8 | 6b | 0.005 | 25 | 90 |
| 7 | 6b | 0.007 | 25 | 88 |

Table 3. The effect of different quantities of the catalyst in model studies. Significant values are in bold.

| Entry | Ar | Ar' | Product | Time (min) | Yield (%) ^a |
|-------|--|---|---------|------------|------------------------|
| 1 | C ₆ H ₅ | C ₆ H ₅ | 4a | 20 | 88 |
| 2 | <i>p</i> -MeC ₆ H ₄ | C ₆ H ₅ | 4b | 15 | 90 |
| 3 | <i>p</i> -MeC ₆ H ₄ | <i>p</i> -ClC ₆ H ₄ | 4c | 15 | 95 |
| 4 | <i>p</i> -MeC ₆ H ₄ | <i>p</i> -OMeC ₆ H ₄ | 4d | 25 | 85 |
| 5 | <i>p</i> -MeC ₆ H ₄ | <i>p</i> -BrC ₆ H ₄ | 4e | 15 | 92 |
| 6 | <i>p</i> -OMeC ₆ H ₄ | C ₆ H ₅ | 4f | 15 | 90 |
| 7 | <i>p</i> -OMeC ₆ H ₄ | <i>p</i> -BrC ₆ H ₄ | 4g | 15 | 95 |
| 8 | <i>p</i> -OMeC ₆ H ₄ | <i>p</i> -OMeC ₆ H ₄ | 4h | 20 | 90 |
| 9 | <i>p</i> -OMeC ₆ H ₄ | <i>p</i> -ClC ₆ H ₄ | 4i | 15 | 97 |
| 10 | <i>p</i> -OMeC ₆ H ₄ | <i>p</i> -CNC ₆ H ₄ | 4j | 15 | 95 |
| 11 | <i>p</i> -OMeC ₆ H ₄ | <i>p</i> -SMcC ₆ H ₄ | 4k | 25 | 88 |
| 12 | <i>p</i> -ClC ₆ H ₄ | C ₆ H ₅ | 4l | 20 | 85 |
| 13 | <i>p</i> -ClC ₆ H ₄ | <i>p</i> -BrC ₆ H ₄ | 4m | 15 | 92 |
| 14 | <i>p</i> -ClC ₆ H ₄ | <i>p</i> -OMeC ₆ H ₄ | 4n | 25 | 85 |
| 14 | C ₆ H ₅ | C ₆ H ₅ | 4n | 30 | 90 |
| 15 | <i>p</i> -MeC ₆ H ₄ | <i>p</i> -MeC ₆ H ₄ | 4o | 35 | 88 |
| 16 | <i>p</i> -MeC ₆ H ₄ | <i>p</i> -BrC ₆ H ₄ | 4p | 25 | 90 |
| 17 | <i>p</i> -MeC ₆ H ₄ | <i>p</i> -ClC ₆ H ₄ | 4q | 25 | 95 |
| 18 | <i>p</i> -MeC ₆ H ₄ | <i>p</i> -OMeC ₆ H ₄ | 4r | 40 | 85 |
| 19 | <i>p</i> -MeC ₆ H ₄ | <i>p</i> -NO ₂ C ₆ H ₄ | 6a | 25 | 95 |
| 20 | <i>p</i> -MeC ₆ H ₄ | <i>p</i> -BrC ₆ H ₄ | 6b | 15 | 90 |
| 21 | <i>p</i> -OMeC ₆ H ₄ | <i>p</i> -CNC ₆ H ₄ | 6c | 30 | 85 |
| 22 | <i>p</i> -OMeC ₆ H ₄ | <i>p</i> -SMcC ₆ H ₄ | 6d | 35 | 90 |

Table 4. Preparation of 1,8-dioxo-decahydro-acridines (4a–r) and 1,8-dioxo-octahydro-xanthenes (6a–d) using IRMOF-3/GO/CuFe₂O₄ under ultrasound irradiations. ^aIsolated yield.

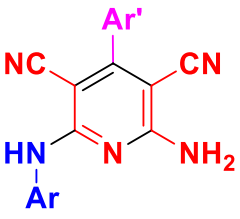
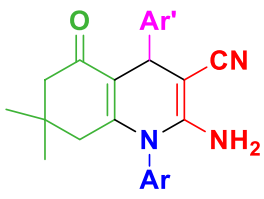
| | Entry | Catalyst | Conditions | Time/yield (%) | References |
|---|-------|---|------------------------|----------------------|------------------|
|  | 1 | ZnCl ₂ | EtOH/Stir.80 °C | 5 h /67–88 | 43 |
| | 2 | DMAPL | MeOH/r.t | 4 h/62–86 | 44 |
| | 3 | ZnCl ₂ /AlCl ₃ /FeCl ₃ | EtOH/Reflux | 6 h/73–95 | 41 |
| | 4 | KOH | EtOH/r.t | 2 h/77–91 | 42 |
| | 5 | IRMOF-3/GO/CuFe₂O₄ | EtOH/ultrasound | 15 min/ 85–97 | This work |
|  | 1 | Piperidine | EtOH/Reflux | 6 h /64–75 | 45 |
| | 2 | [bmim ⁺][BF ₄ ⁻] | Stir.(90 °C) | 5 h/94–99 | 46 |
| | 3 | MNP@BSAT@Cu(OAc) ₂ | EtOH/r.t | 25 min/80–94 | 47 |
| | 4 | Zr(HPO ₄) ₂ | Solvent-free/80 °C | 2 h/65–98 | 48 |
| | 5 | IRMOF-3/GO/CuFe₂O₄ | EtOH/ultrasound | 15 min/85–95 | This work |

Table 5. Comparison of the outcomes of the production of 2-amino-4-aryl-6-substituted pyridine-3,5-dicarbonitrile and hydroquinoline-3-carbonitrile derivatives by means of different catalysts. Significant values are in bold.

indicated, there is no considerable differences between X-ray diffraction of the fresh IRMOF-3/GO/CuFe₂O₄ and the recovered catalyst, confirming the good stability of the prepared nanocatalyst after 7 runs (Fig. 7).

Figure 8 shows a reasonable mechanism for synthesizing pyridine derivatives (4a–4r) catalyzed by IRMOF-3/GO/CuFe₂O₄. This result is, supported by previous studies^{41,42}. IRMOF-3/GO/CuFe₂O₄ was assumed to serve as Lewis acids that causes increasing electrophilicity of the carbonyl groups, double and triple bonds in substrates and intermediate via a strong coordination bond^{17,49}. Initially, the mechanistic approach includes the Knoevenagel condensation of aromatic aldehyde and malononitrile, creating adduct I. Then, adding anilines to intermediate I was followed by involving malononitrile to make intermediate II. Tautomerization and intramolecular cyclization on intermediate II produced intermediate III with a dihydropyridine moiety.

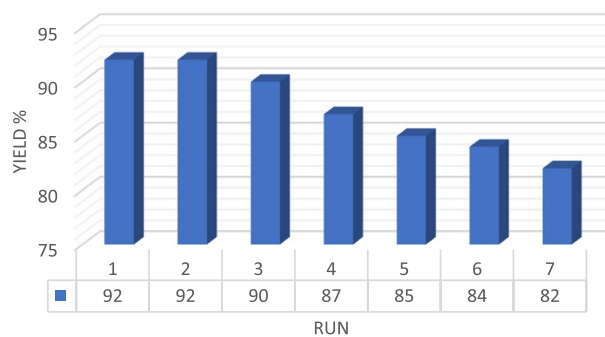


Figure 6. Reusability of the IRMOF-3/GO/CuFe₂O₄ catalyst.

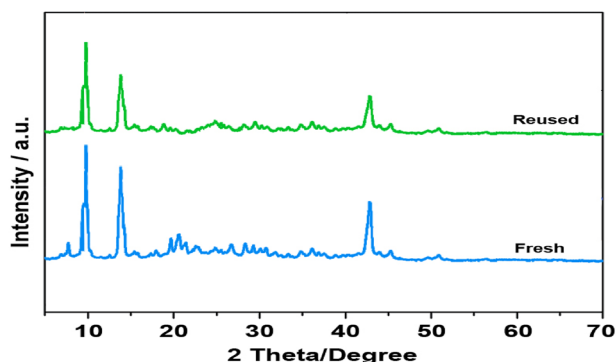


Figure 7. XRD pattern of the recovered IRMOF-3/GO/CuFe₂O₄.

Finally, 2-amino-6-alkylamino-3,5-dicyanopyridines **4** was prepared by aromatization of intermediate **III**. Additionally, the catalytic behavior of IRMOF-3/GO/CuFe₂O₄ on the quinoline synthesis was identical to the described mechanism for synthesizing pyridine derivatives.

Conclusion

The present work aimed to present a convenient and facile technique to prepare magnetic copper ferrite nanoparticles supported on IRMOF-3/GO. This magnetic heterogeneous and reusable nano catalyst to prepare heterocyclic compounds via the reactions between of various aromatic aldehydes, malononitrile, diverse primary amines and dimedone under ultrasound irradiations. The methods for characterizing the IRMOF-3/GO/CuFe₂O₄ were SEM, BET, FT-IR, XRD, TGA, and EDX. It was indicated that this catalyst is effective for synthesis of pyridines and quinoline derivatives. Moreover, this technique has good benefits like eco-friendly, higher performance and a very convenient working technique.

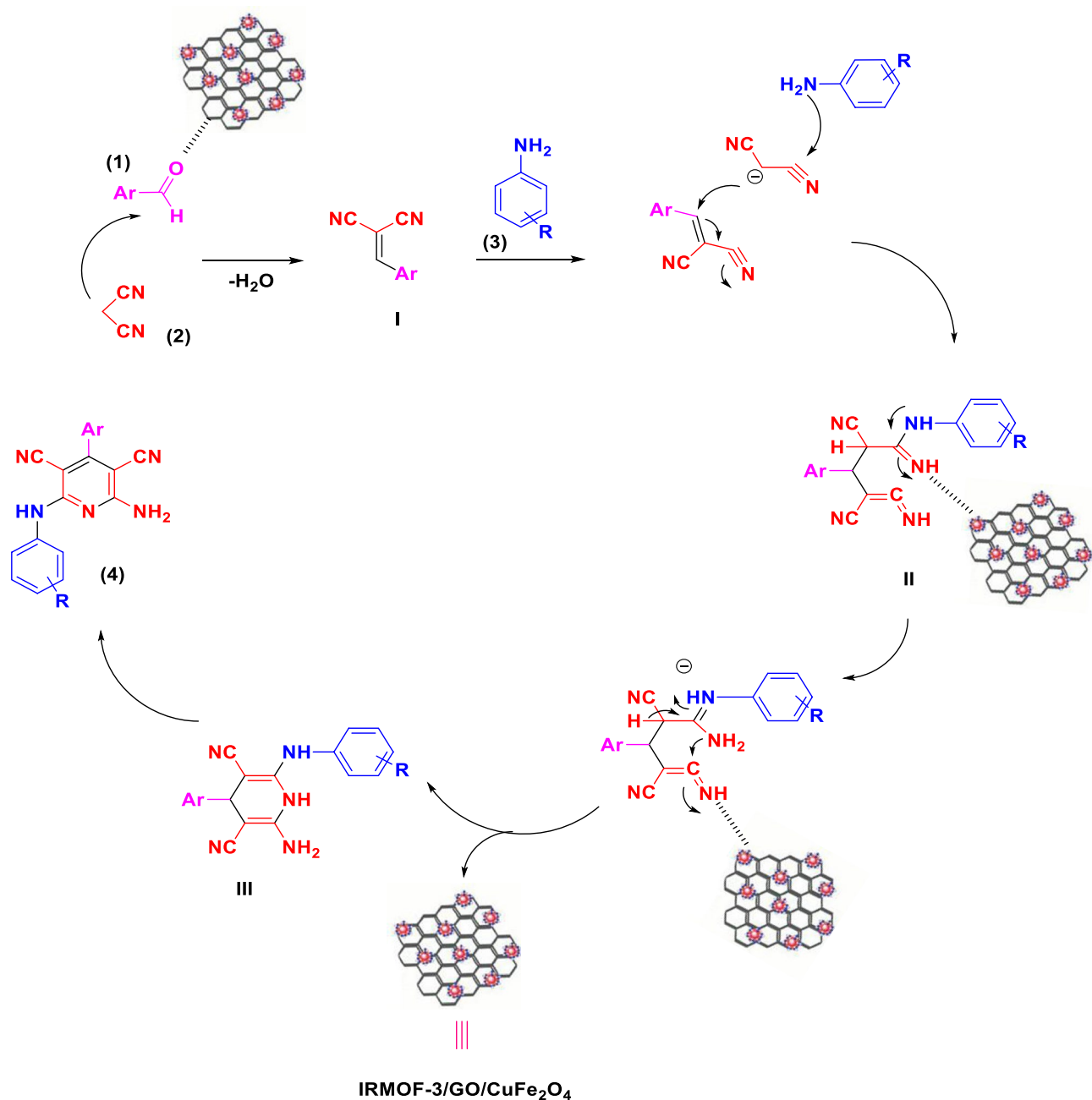


Figure 8. The proposed mechanism to synthesize pyridine derivatives using IRMOF-3/GO/CuFe₂O₄.

Data availability

All data generated or analyzed during this study are included in this published article [and its supplementary information file].

Received: 21 September 2022; Accepted: 30 May 2023

Published online: 05 June 2023

References

1. Yang, W. *et al.* Graphene oxide-based noble-metal nanoparticles composites for environmental application. *Compos. Commun.* **24**, 100645 (2021).
2. Sultana, S., Bordoloi, S., Konwer, S., Borah, G. & Gogoi, P. K. Reduced graphene oxide/iron oxide hybrid composite material as an efficient magnetically separable heterogeneous catalyst for transfer hydrogenation of ketones. *Appl. Organomet. Chem.* **34**, e5582 (2020).
3. Chen, Y., Zhu, Q., Tsumori, N. & Xu, Q. Immobilizing highly catalytically active noble metal nanoparticles on reduced graphene oxide: A non-noble metal sacrificial approach. *J. Am. Chem. Soc.* **137**, 106 (2015).
4. Mittal, A., Kumari, S., Parmanad, D. & Yadav, S. K. A new copper complex on graphene oxide: A heterogeneous catalyst for N-arylation and C-H activation. *Appl. Organomet. Chem.* **34**, e5362 (2020).

5. Yun, Y. *et al.* Design and remarkable efficiency of the robust sandwich cluster composite nanocatalysts ZIF-8@Au₂₅@ZIF-67. *J. Am. Chem. Soc.* **142**, 4126 (2020).
6. Lee, J. *et al.* Metal-organic framework materials as catalysts. *Chem. Soc. Rev.* **38**, 1450 (2009).
7. Hanifehpour, Y., Dadashi, J. & Mirtamizdoust, B. The synthesis and characterization of a novel one-dimensional bismuth (III) coordination polymer as a precursor for the production of bismuth (III) oxide nanorods. *Crystals* **11**, 197 (2021).
8. Bavykina, A. *et al.* Metal-organic frameworks in heterogeneous catalysis: recent progress, new trends, and future perspectives. *Chem. Rev.* **120**, 8468 (2020).
9. Dadashi, J. *et al.* The synthesis and characterization of a novel one-dimensional bismuth (III) coordination polymer as a precursor for the production of bismuth (III) oxide nanorods. *Crystals* **11**, 682 (2021).
10. Baumann, A. E., Burns, D. A., Liu, B. & Thoi, V. S. Metal-organic framework functionalization and design strategies for advanced electrochemical energy storage devices. *Commun. Chem.* **2**, 86 (2019).
11. Liang, Z., Zhao, R., Qiu, T., Zou, R. & Xu, Q. Metal-organic framework-derived materials for electrochemical energy applications. *Energy Chem.* **1**, 100001 (2019).
12. Sun, Y. *et al.* Metal-organic framework nanocarriers for drug. *Nano-Micro Lett.* **12**, 103 (2020).
13. Ghasemzadeh, M. A., Eshkevari, B. M., Tavakoli, M. & Zamani, F. Metal-organic frameworks: Advanced tools for multicomponent reactions. *Green Chem.* **22**, 7265 (2020).
14. Chen, L. & Xu, Q. Metal-organic framework composites for catalysis. *Matter.* **1**, 57 (2019).
15. He, S. *et al.* Metal-organic frameworks for advanced drug delivery. *Acta Pharm. Sin. B.* **11**, 2362 (2021).
16. Guo, X. *et al.* Band gap engineering of metal-organic frameworks for solar fuel productions. *Coord. Chem. Rev.* **435**, 213785 (2021).
17. Aguirre-Diaz, M. *et al.* Tunable catalytic activity of solid solution metal-organic frameworks in one-pot multicomponent reactions. *J. Am. Chem. Soc.* **137**, 6132 (2015).
18. Domling, A., Wang, W. & Wang, K. Chemistry and biology of multicomponent reactions. *Chem. Rev.* **112**, 3083 (2012).
19. Esfahani, M. N., Hoseini, S. J., Montazerzohori, M., Mehrabi, R. & Nasrabadi, H. Magnetic Fe₃O₄ nanoparticles: Efficient and recoverable nanocatalyst for the synthesis of polyhydroquinolines and Hantzsch 1,4-dihydropyridines under solvent-free conditions. *J. Mol. Catal. A* **382**, 99 (2014).
20. Yadav, D., Patel, R., Srivastava, V., Watal, G. & Yadav, L. LiBr as an efficient catalyst for one-pot synthesis of hantzsch 1,4-dihydropyridines under mild conditions. *Chin. J. Chem.* **29**, 118 (2011).
21. Xia, J. J. & Zhang, K. H. Synthesis of *N*-substituted acridinediones and polyhydroquinoline derivatives in refluxing water. *Molecules* **17**, 5339 (2012).
22. Sarkar, R. & Mukhopadhyay, C. Cross-dehydrogenative regioselective Csp³-Csp² coupling of enamino-ketones followed by rearrangement: An amazing formation route to acridine-1,8-dione derivatives. *Org. Biomol. Chem.* **14**, 2706 (2016).
23. Khodja, I. A. *et al.* Solvent-free synthesis of dihydropyridines and acridinediones via a salicylic acid-catalyzed hantzsch multicomponent reaction. *Synth. Commun.* **44**, 959 (2014).
24. Karade, N. N., Budhewar, V. H., Shinde, S. V. & Jadhav, W. N. L-proline as an efficient organo-catalyst for the synthesis of polyhydroquinoline via multicomponent Hantzsch reaction. *Lett. Org. Chem.* **4**, 16 (2007).
25. Kagne, R. P., Nikam, G. H., Kalalawe, V. G., Niwadange, S. N. & Munde, D. R. An efficient protocol for synthesis of 1,4-dihydropyridine derivatives by using graphene oxide nano particles as a catalyst. *J. Chem. Sci.* **7**, 1064 (2017).
26. Safaei-Ghomi, J., Zahedi, S. & Ghasemzadeh, M. A. ChemInform Abstract: AgI nanoparticles as a remarkable catalyst in the synthesis of (Amidoalkyl)naphthol and oxazine derivatives: An eco-friendly approach. *Monatsh. Chem.* **145**, 1191 (2014).
27. Ghasemzadeh, M. A., Eshkevari, B. M. & Abdollahi-Basir, M. H. MIL-53(Fe) metal-organic frameworks (MOFs) as an efficient and reusable catalyst for the one-pot four-component synthesis of pyrano[2,3-*c*]pyrazoles. *Appl. Organomet. Chem.* **33**, e4679 (2019).
28. Abdollahi-Basir, M. H., Mirhosseini-Eshkevari, B., Zamani, F. & Ghasemzadeh, M. A. Synthesis of tetrazolo[1,5-*a*]pyrimidine-6-carbonitriles using HMTA-BAIL@MIL-101(Cr) as a superior heterogeneous catalyst. *Sci. Rep.* **11**, 5109 (2021).
29. Xu, Y. *et al.* Multifunctional Fe₃O₄@C-based nanoparticles coupling optical/MRI imaging and pH/photothermal controllable drug release as efficient anti-cancer drug delivery platforms Nanotechnology. *Nanotechnology* **30**, 1 (2019).
30. Naeimi, H. & Golestanzadeh, M. Highly sulfonated graphene and graphene oxide nanosheets as heterogeneous nanocatalysts in green synthesis of bisphenolic antioxidants under solvent free conditions. *RSC Adv.* **4**, 56475 (2014).
31. Ghasemzadeh, M. A., Mirhosseini-Eshkevari, B. & Dadashi, J. IRMOF-3 functionalized GO/CuFe₂O₄: A new and recyclable catalyst for the synthesis of dihydropyrano[2,3-*c*]pyrazoles under ultrasound irradiations. *J. Mol. Struct.* **1261**, 132843 (2022).
32. Nemat, F., Elhampour, A., Farrokhi, H. & Natanzi, M. B. Cu₂O/nano-CuFe₂O₄: A novel and recyclable magnetic catalyst for three-component coupling of carbonyl compounds-alkynes-amines under solvent-free condition. *Catal. Commun.* **66**, 15 (2015).
33. Emam, H. E., El-Shahat, M., Taha, M. & Abdelhameed, R. M. Microwave assisted post-synthetic modification of IRMOF-3 and MIL-68-NH₂ onto cotton for Fuel purification with computational explanation. *Surf. Interfaces* **30**, 101940 (2022).
34. Petit, C. & Bandoz, T. J. MOF-graphite oxide nanocomposites: Surface characterization and evaluation as adsorbents of ammonia. *J. Mater. Chem.* **19**, 6521 (2009).
35. Hassanzadeh-Afruzi, F., Bahrami, S. & Maleki, A. ZnS/CuFe₂O₄: Magnetic hybrid nanocomposite to catalyze the synthesis of 2,4,5-triaryl-1H-imidazole derivatives. *Proceedings* **41**, 44 (2019).
36. Rathod, V. N., Bansode, N. D., Thombre, P. B. & Lande, M. K. Efficient one-pot synthesis of polyhydroquinoline derivatives through the Hantzsch condensation using IRMOF-3 as heterogeneous and reusable catalyst. *J. Chin. Chem. Soc.* **68**, 601 (2021).
37. Lin, J. *et al.* Fabrication of GO@MIL-101(Fe) for enhanced visible-light photocatalysis degradation of organophosphorus contaminant. *J. Water Proc. Eng.* **33**, 101010 (2020).
38. Tabatabaeian, K., Zanjanchi, M. A., Mahmoodi, N. O. & Eftekhari, T. Anchorage of a ruthenium complex into modified MOF: Synergistic effects for selective oxidation of aromatic and heteroaromatic compounds. *RSC Adv.* **5**, 101013 (2015).
39. Allen, C. A. *et al.* Chemically crosslinked isoreticular metal-organic frameworks. *Chem. Commun.* **49**, 3200 (2013).
40. Lopez, K. S. *et al.* Assessment of nutritive value of cereal and legume straws based on chemical composition and in vitro digestibility. *J. Sci. Food Agric.* **85**, 1550 (2005).
41. Mahmoud, N. F. H. & El-Sewedy, A. Multicomponent reactions, solvent-free synthesis of 2-amino-4-aryl-6-substituted pyridine-3,5-dicarbonitrile derivatives, and corrosion inhibitors evaluation. *J. Chem.* **1**, 1 (2018).
42. Khan, M. N., Pal, S., Parvin, T. & Choudhury, L. H. A simple and efficient method for the facile access of highly functionalized pyridines and their fluorescence property studies. *RSC Adv.* **2**, 12305 (2012).
43. Huang, J. *et al.* A new and efficient ZnCl₂-catalyzed synthesis and biological evaluation of novel 2-amino-3,5-dicyano-4-aryl-6-aryl-aminopyridines as potent antibacterial agents against *Helicobacter pylori* (HP). *Tetrahedron* **71**, 8628 (2015).
44. Sarkar, S., Das, D. K. & Khan, A. T. Synthesis of fully-substituted pyridines and dihydropyridines in a highly chemoselective manner utilizing a multicomponent reaction (MCR) strategy. *RSC Adv.* **4**, 53752 (2014).
45. Ghoneim, A. & Assy, M. G. Synthesis of some new hydroquinoline and pyrimido[4,5-*b*]quinoline derivatives. *Curr. Res. Chem.* **7**, 14 (2015).
46. Wang, X. S., Zhang, M. M., Jiang, H., Yao, C. S. & Tu, S. J. Three-component green synthesis of *N*-arylquinoline derivatives in ionic liquid [Bmim⁺][BF₄⁻]: reactions of arylaldehyde, 3-arylamino-5,5-dimethylcyclohex-2-enone, and active methylene compounds. *Tetrahedron* **63**, 4439 (2007).

47. Ahadi, N., Mobinikhaledi, A. & Bodaghifard, M. A. One-pot synthesis of 1,4-dihydropyridines and N-arylquinolines in the presence of copper complex stabilized on MnFe_2O_4 (MFO) as a novel organic–inorganic hybrid material and magnetically retrievable catalyst. *Appl. Organomet. Chem.* **34**, e5822 (2020).
48. Abdolmohammadi, S. Study of the catalytic activity of $\text{Zr}(\text{HPO}_4)_2$ in the synthesis of hexahydroquinoline derivatives under solvent-free conditions. *Z. Naturforsch.* **68**, 195 (2013).
49. Park, J. *et al.* Ultra-large-scale syntheses of monodisperse nanocrystals. *Nat. Mater.* **3**, 891 (2004).

Acknowledgements

The author gratefully acknowledges the financial support of this work by the Research Affairs Office of the Islamic Azad University, Qom Branch, Qom, I. R. Iran [Grant Number 2019-2898].

Author contributions

M.A.G. and J. D. wrote the main manuscript and B.M.-E. prepared figures. All authors reviewed the manuscript.

Competing interests

The authors declare no competing interests.

Additional information

Supplementary Information The online version contains supplementary material available at <https://doi.org/10.1038/s41598-023-36115-2>.

Correspondence and requests for materials should be addressed to M.A.G.

Reprints and permissions information is available at www.nature.com/reprints.

Publisher's note Springer Nature remains neutral with regard to jurisdictional claims in published maps and institutional affiliations.



Open Access This article is licensed under a Creative Commons Attribution 4.0 International License, which permits use, sharing, adaptation, distribution and reproduction in any medium or format, as long as you give appropriate credit to the original author(s) and the source, provide a link to the Creative Commons licence, and indicate if changes were made. The images or other third party material in this article are included in the article's Creative Commons licence, unless indicated otherwise in a credit line to the material. If material is not included in the article's Creative Commons licence and your intended use is not permitted by statutory regulation or exceeds the permitted use, you will need to obtain permission directly from the copyright holder. To view a copy of this licence, visit <http://creativecommons.org/licenses/by/4.0/>.

© The Author(s) 2023